J Mater Sci: Mater Electron (2016) 27:2504–2510
DOI 10.1007/s10854-015-4051-7

Synthesis and characterization of flower-like ZnO structures and their applications in photocatalytic degradation of Rhodamine B dye

N. Rana[1] · Subhash Chand[1] · Arvind K. Gathania[1]

Received: 14 August 2015 / Accepted: 6 November 2015 / Published online: 14 November 2015

Abstract We have synthesized ZnO nanoflakes (ZnO-NFs) assembled flower-like structures through simple wet chemical route without using any growth directing agent. The ZnO NFs have been characterized in terms of morphological, structural, and optical properties by field emission-scanning electron microscope (FE-SEM), X-ray diffraction (XRD), Raman, Fourier transform infrared (FTIR) and ultraviolet–visible (UV–Vis) spectroscopy. FE-SEM images show the nanoflakes assembled flower-like morphology of the as-prepared sample. XRD and Raman studies confirm that it has stable wurtzite structure. The formation of ZnO-NFs is also confirmed by the bond corresponding to metal-oxygen vibration in the FTIR spectrum at $\sim$460 cm^{-1}. The UV–Vis absorption spectrum of synthesized sample gives the optical band gap value of 3.2 eV. The photocatalytic activity of the ZnO-NFs is evaluated by observing their role in the photocatalytic degradation of Rhodamine B (RhB) dye. Results show that ZnO-NFs are capable of working efficiently for the degradation of RhB dye.

1 Introduction

ZnO is a most versatile multifunctional n-type semiconductor because of its wide direct band gap (3.35 eV at 300 K), high exciton binding energy (60 meV), high melting point, excellent radiation hardness and piezoelectric properties [1]. ZnO nanostructures have promising applications in photocatalysis, solar cells, optical waveguides, sensors, and nano-generator [2–8] etc. Among these applications, the photocatalytic activity has received much attention of researchers and widely studied because of its characteristic features such as, easy tuning to various surface morphologies [3, 9–13], low temperature sample processing, high defects, high quantum yield for peroxide production and low cost [14–24]. Photocatalysis involves the generation of active species upon illumination of aqueous suspensions of semiconductor with the light of suitable wavelength. These active species are proficient in carrying out the destruction of organic pollutants [25, 26]. ZnO nanostructures with different morphologies can be synthesized by various synthesis routes such as sol–gel, precipitation, solvothermal, electrodeposition, mechanochemical and sonochemical [27–33] etc. Xie et al. [3] have reported that the sheet –like structures of ZnO exhibit better photocatalytic activities as compared to its spherical structure. Wang et al. [10] have prepared ZnO with flowers and rods like morphologies and concluded that ZnO nanoflowers show the higher photocatalytic activity than that of ZnO nanorods. Sun et al. [9] have obtained ZnO-3D hierarchical structures of ZnO assembled by nanosheet, nanoneedle and found that flower shaped sample exhibits an enhanced photocatalytic performance as compared with the nanosheet, nanoneedle structures. In the present investigation, we have reported the synthesis, characterization and photocatalytic activity of hierarchically assembled architectures of ZnO-NFs obtained by the wet chemical method without the use of any surfactant or capping agent. The photocatalytic activity is systematically studied by observing the degradation of Rhodamine B (RhB) dye.

2 Experimental

2.1 Materials used

Zinc acetate dihydrate [$Zn(CH_3COO)_2{\cdot}2H_2O$-Purity $\geq$ 98 %] is obtained from Merck-India. Methanol is

✉ Arvind K. Gathania
akgathania@yahoo.com

[1] Department of Physics, National Institute of Technology-Hamirpur, Hamirpur, H.P. 177 005, India

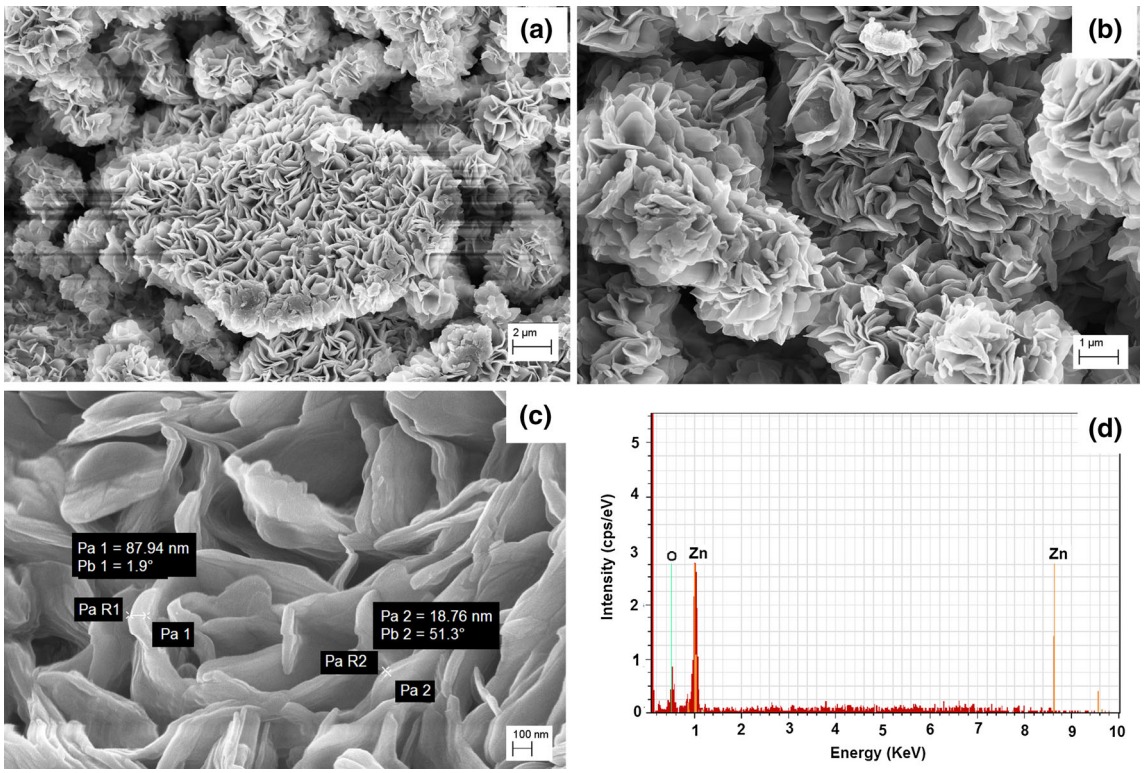

Fig. 1 **a–c** FE-SEM images and **d** EDX spectrum of wet chemical route synthesized ZnO-NFs

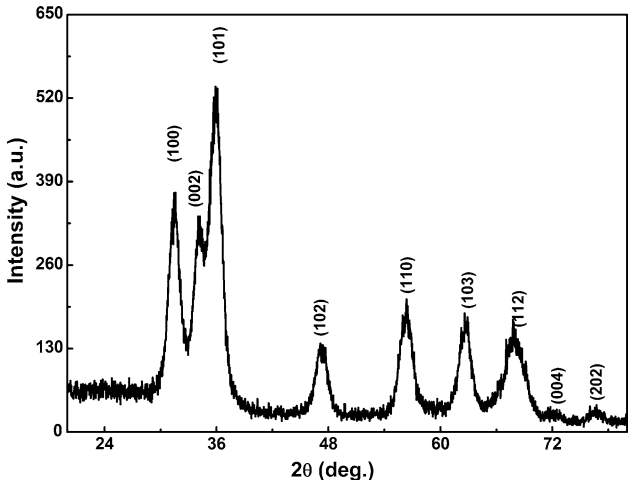

Fig. 2 XRD pattern of wet chemical route synthesized ZnO-NFs

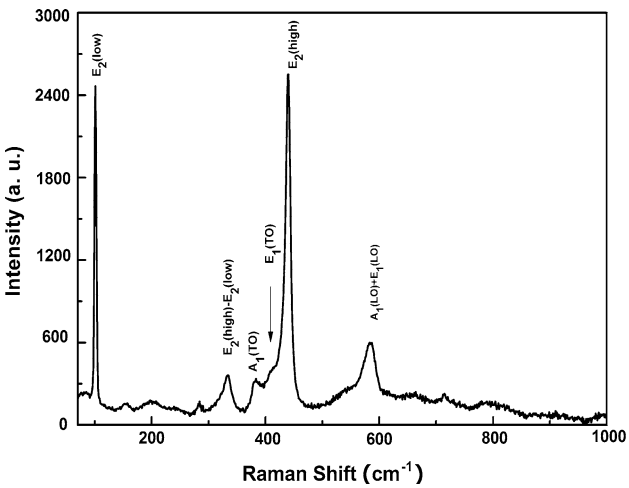

Fig. 3 Raman spectra of the as-synthesized ZnO-NFs

purchased from Sigma-Aldrich (CH_3OH-Purity $\geq$ 99 %) and Lithium hydroxide (LiOH-Purity = 99 %) is purchased from Otto. RhB dye is obtained from Fisher scientific (Purity $\geq$ 99 %). All the chemicals are used without further purification.

2.2 Preparation of ZnO-NFs

A 0.25 M solution of $Zn(CH_3COO)_2{\cdot}2H_2O$ is prepared in 100 ml methanol and refluxed at about 70 °C for 30 min under magnetic stirring to get a well-mixed solution. For hydrolysis, 0.25 M solution of LiOH in 100 ml methanol is added dropwise to it. The resulting solution is refluxed at 70 °C under continuous stirring for 2 h to complete precipitation process. The reacted mixture is then kept for some time and the clear solution is decanted. Finally, the precipitates are washed, filtered and dried in vacuum oven for 24 h and used for further characterization.

2.3 Characterization

The morphology and elemental investigations are carried out using Field emission-scanning electron microscope (FE-SEM, SIGMA HV—Carl Zeiss) equipped with energy dispersive X-ray analysis (EDX) Bruker machine. The crystal structure of the synthesized sample is investigated by X-ray diffraction (XRD, X'Pert Pro, Philips) with Cu-K_α radiation ($\lambda = 1.5406$ Å). The characteristic functional groups are investigated using Fourier transform infrared (FTIR PerkinElmer Spectrum 65) spectrophotometer. Raman study is performed with an InVia Raman spectrophotometer (Renishaw) with Ar^+ ion laser beam having a wavelength of 514 nm. The Optical properties are determined by Ultraviolet–visible (UV–Vis) spectrometer (PerkinElmer, LAMBDA 750).

The photocatalytic activity of the as-prepared ZnO-NFs is investigated by the degradation of RhB under UV irradiation at room temperature. Prior to irradiation, the aqueous suspension of RhB and ZnO-NFs powder is stirred in dark for 30 min to establish the adsorption–desorption equilibrium and then irradiated under the 30 W UV lamp. A series of samples are taken out after a regular time interval and centrifuged to remove the suspended ZnO-NFs and analyzed by a UV–Vis spectrophotometer to obtain the absorbance of the RhB solutions.

The degradation efficiency X (%) is calculated from absorption spectra using the following relation:

$$X\,(\%) = \frac{(A_0 - A_t)}{A_0} \times 100, \quad (1)$$

where A_0 represents the initial absorbance and A_t is the absorbance at certain time t. The photocatalytic degradation reaction of RhB follows pseudo-first order kinetics and the rate constant is determined by the following relation:

$$\ln\left(\frac{C_0}{C_t}\right) = k \times t = \ln\left(\frac{A_0}{A_t}\right), \quad (2)$$

The rate constant k is calculated from the slope of straight line portion of $\ln(A_0/A_t)$ versus t plot.

3 Results and discussion

Figure 1a–c shows the FE-SEM images of synthesized ZnO-NFs assembled flowers taken at the different resolution. The images clearly reveal that these nanoflakes have the thickness of below 100 nm range and are grown upward to form flower-like morphology.

The Fig. 1d shows the EDX spectrum of ZnO-NFs. It clearly confirms the presence of zinc and oxygen elements in the sample. No peaks belonging to any other element is found in the spectrum, which confirms that the prepared sample is free from impurity.

Figure 2 shows XRD pattern of the wet chemical route synthesized ZnO-NFs. All the diffraction peaks are well matched and can be indexed as the hexagonal wurtzite ZnO as reported in standard diffraction data (JCPDS card No.: 36-1451).

Figure 3 shows the Raman spectra of the as-prepared ZnO sample. For wurtzite ZnO (space group P63mc) near the center of the Brillouin zone (k = 0), group theory predicts the existence of the following optical modes: $\Gamma opt = A_1 + E_1 + 2E_2 + 2B_1$. The B_1 modes are silent,

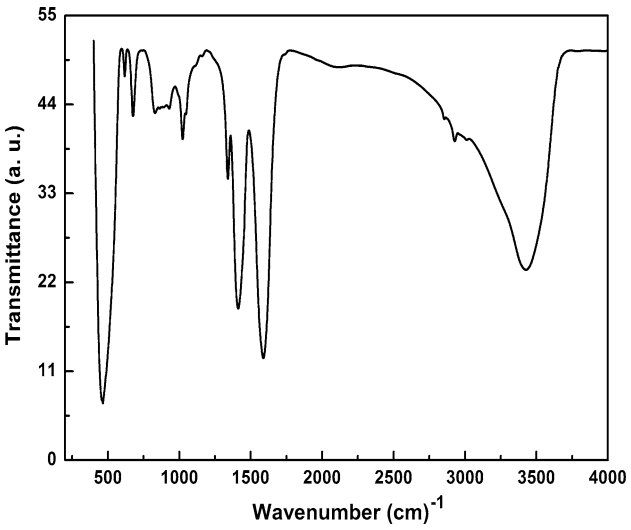

Fig. 4 FTIR spectrum of wet chemical route synthesized ZnO-NFs

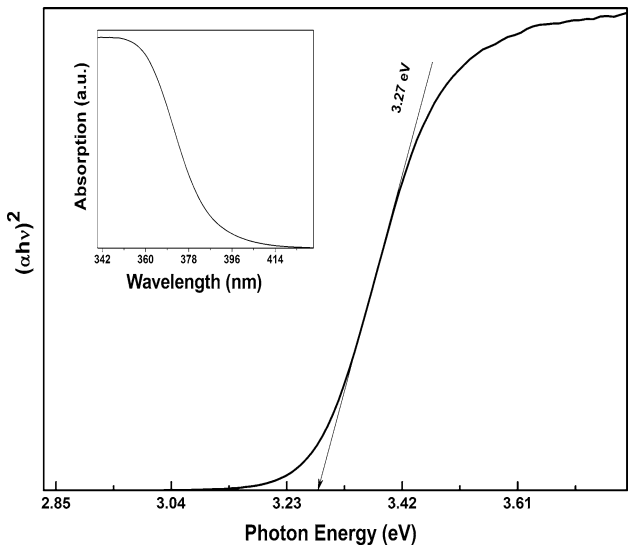

Fig. 5 Tauc's plot of wet chemical route synthesized ZnO-NFs. The *inset* shows UV–Vis absorption spectrum of ZnO-NFs

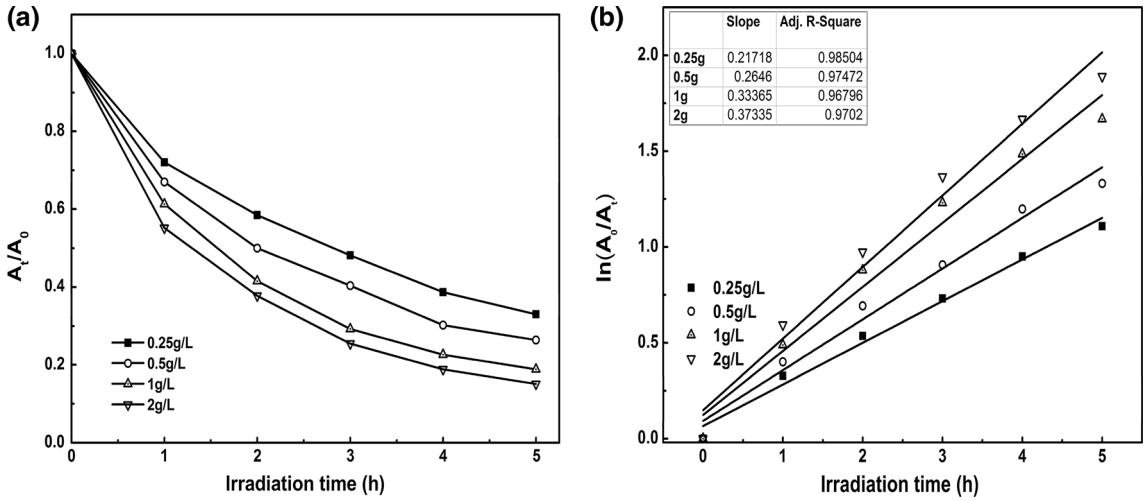

Fig. 6 **a** The photodegradation time profile and **b** the first-order kinetic model fit for the photodegradation of RhB solution (RhB concentration: 5 ppm) in the presence of different ZnO-NFs loading (0.25–2.0 g/L)

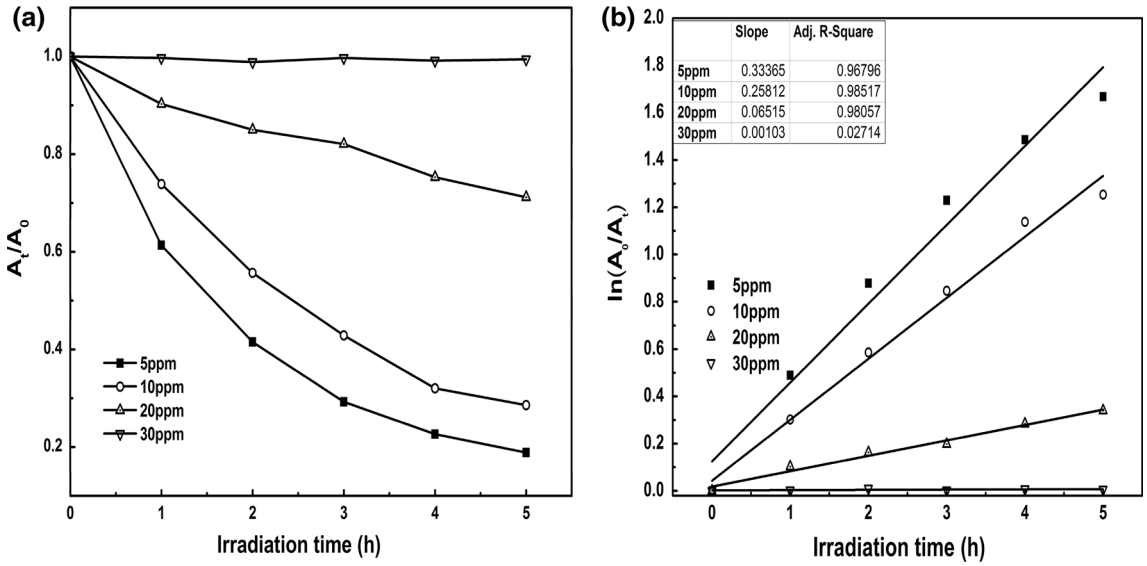

Fig. 7 **a** The photodegradation time profile and **b** the first-order kinetic model fit for the photodegradation of RhB solution (RhB concentration: 5–30 ppm) in the presence of ZnO-NFs (1 g/L) photocatalyst

the E_2 modes are non-polar and Raman active, while A_1 and E_1 are polar modes and Raman as well as infrared active [34].

The two dominant peaks at around 101 and 439 cm^{-1} are characteristic peaks of the wurtzite ZnO and are assigned to the low- and high-E_2 mode. The peaks around 385 and 413 cm^{-1} are attributed to the A_1(TO) mode and E_1(TO) modes, respectively. A smaller peak around 334 cm^{-1} is attributed to a [E_2(high) − E_2(low)] mode. The Raman peak located around 583 cm^{-1} corresponds to $A_1 + E_1$ symmetry with LO modes. The presence of high intensity of E_2 modes represents the good quality of ZnO nanomaterials, which is consistent with XRD result. Figure 4 shows the FTIR spectrum of prepared ZnO-NFs. It illustrates a series of absorption bands in the range of 450–4000 cm^{-1}. The broad absorption band observed at ~3300 cm^{-1} is assigned to the O–H stretching mode for –COOH group in zinc acetate and H_2O molecule. Two absorption bands at ~2880 and ~2940 cm^{-1} correspond to the C–H stretching vibrations of acetate. The bands appearing between ~1400 and 1600 cm^{-1} are due to the stretching modes (symmetric and asymmetric) of the acetate group (–COOH). The absorption band at ~1000 cm^{-1} is due to the C=O deformation mode. These groups are believed to be adsorbed on the surface of the nanoparticles during

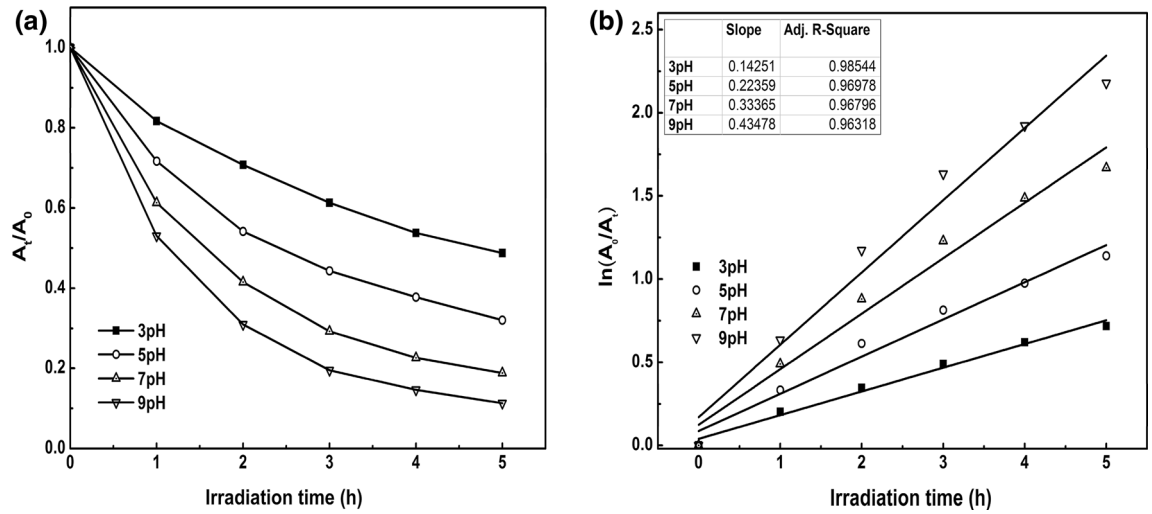

Fig. 8 **a** The photodegradation time profile and **b** the first-order kinetic model fit for the photodegradation of RhB solution (RhB concentration: 5 ppm and ZnO-NFs concentration: 1 g/L) with different solution pH

Table 1 Effect of photocatalyst loading, initial RhB concentration and solution pH on the photocatalytic activities of ZnO-NFs

ZnO loading (g/L)	k (h^{-1})	X (%)	Initial RhB concentration (ppm)	k (h^{-1})	X (%)	Initial solution pH	k (h^{-1})	X (%)
0.25	0.2171	66	5	0.3336	81	3	0.1425	57
0.50	0.2646	73	10	0.2581	71	5	0.2235	68
1.00	0.3336	81	20	0.0651	28	7	0.3336	81
2.00	0.3733	85	30	0.0010	1	9	0.4347	88

the synthesis process. The band positioned at $\sim$460 cm^{-1} is associated with the characteristic wurtzite lattice vibrations (Zn–O) [35, 36].

The optical band gap of the ZnO-NFs sample is estimated using the Tauc's equation which demonstrates a relationship between absorption coefficient (α) and the incident photon energy ($h\nu$) as follows [37]:

$$(\alpha h\nu) = A(h\nu - E_g)^n \quad (3)$$

Figure 5 shows the $(\alpha h\nu)^2$ versus $h\nu$ plot using the data from optical absorbance spectra. An extrapolation of the linear portion of the plot onto the x-axis $[(\alpha h\nu)^2 = 0]$ gives the value of E_g. The calculated value of optical band gap is 3.22 eV.

3.1 Photocatalytic activity

The underlying mechanism of the photocatalytic degradation of RhB by the ZnO-NFs under irradiation can be explained on the basis of photogeneration of electron–hole pairs (excitons) in ZnO-NFs. The photo-generated charge carriers move freely on the surface of the ZnO-NFs and initiate redox reactions with water (H_2O) and oxygen (O_2) molecules. The holes in the valence band can act as the site for strong oxidation. They oxidize H_2O molecules and hydroxyl (OH^-) groups to generate highly reactive hydroxyl ($OH^{\cdot}$) radical and H^+ ion. O_2 molecules adsorbed on the surface is reduced by the electrons in the conduction band to form superoxide anion ($O_2^{\cdot -}$) radicals, which react with H^+ to generate hydrogen peroxide ($HO_2^{\cdot}$) radicals. These $HO_2^{\cdot}$ radicals react with electrons and H^+ ions to produce molecules of H_2O_2. In addition, the intrinsic crystal defects (O-vacancies, Zn-interstitial) in the ZnO crystals act as electron donors. These additional electrons from the intrinsic crystal defects further promote the reactions to yield $OH^{\cdot}$ radicals. These highly reactive species $OH^{\cdot}$ radicals and H_2O_2 molecules have the strong oxidative potential for partial or complete decomposition of various organic, inorganic and microbial contaminants adsorbed on the photocatalyst surface [38–40]. The temporal degradation and kinetics of photocatalytic activity of batches of solutions with different ZnO, dye concentration and pH of the solution are presented in Figs. 6, 7 and 8, respectively. From Fig. 6 it is observed that the degradation of dye increases with the increase in the ZnO loading from 0.25 to 2.0 g/L for a fixed value of RhB concentration

(5 ppm). This is attributed to the increase in the availability of reaction sites for the photocatalytic reactions with the increase in the ZnO loading. The increase in the reaction sites creates more hydroxyl radicals with UV irradiation which results in the degradation of more dye molecules.

Figure 7 represents the effect of the initial RhB concentration ranging from 5 to 30 ppm, on the photodegradation efficiency of ZnO-NFs. This shows that for a fixed load of ZnO (1.0 g/L), the rate of dye degradation decreases with the increase in the RhB initial concentration. It is due to the decrease in the both the availability of reaction sites and the path length of the photons entering into the solution. As the path length of photons entering into the solution decreases fewer photons reach the catalyst surface, which results in the decrease in the generation reactive hydroxyl and superoxide radicals.

Figure 8 shows the effect of solution pH on photocatalytic degradation of RhB. The pH of the solution is varied from 3.0 to 9.0 for fixed concentration of ZnO (1 g/L) and RhB (5 ppm). It is observed that the RhB photodegradation enhances with the increase in the pH of the solution. This is because, at high pH value, the presence of large quantities OH ions favours the formation of more hydroxyl radical and, therefore, increases the photodegradation of RhB.

Table 1 summarizes the calculated degradation efficiency and the rate constant with different catalyst loading, initial RhB concentration and solution pH. It represents that the degradation efficiency and the rate of degradation of RhB are more with the increase in the ZnO-NFs loading and the pH of the solution, whereas lowering with the increase in the concentration of RhB in the solution. These variations are attributed to the change in the in the availability of highly reactive species ($OH^{\cdot}$ radicals and H_2O_2 molecules) with the change in the photocatalyst loading, dye concentration and pH of the solution values.

4 Conclusion

Flower-like ZnO-NFs structures have been synthesized successfully by simple wet chemical route without using any surfactant or capping agent. The formation of ZnO is confirmed by XRD, Raman, FT-IR and UV–Vis spectroscopy measurements. The photocatalytic study demonstrates an effective photodegradation of RhB dye by ZnO-NFs. These results suggest that as-synthesized ZnO flower-like structures can be employed as potential semiconductor photocatalyst for applications in wastewater treatment. Moreover, these ZnO flowers for their larger accessible surface area are also expected to be useful for other practical applications such as solar cells, sensors, and optical devices etc.

Acknowledgments Authors thank NIT Hamirpur for providing financial assistance to carry out the present work. Authors also thank CMSE NIT-Hamirpur for providing experimental facilities.

References

1. Ü. Özgür, Y.I. Alivov, C. Liu, A. Teke, M.A. Reshchikov, S. Doğan et al., A comprehensive review of ZnO materials and devices. J. Appl. Phys. **98**, 1–103 (2005)
2. N. Rana, S. Chand, A.K. Gathania, Band gap engineering of ZnO by doping with Mg. Phys. Scr. **90**, 085502 (1–6) (2015)
3. J. Xie, H. Wang, M. Duan, L. Zhang, Synthesis and photocatalysis properties of ZnO structures with different morphologies via hydrothermal method. Appl. Surf. Sci. **257**, 6358–6363 (2011)
4. J.A. Anta, E. Guillén, R. Tena-Zaera, ZnO-based dye-sensitized solar cells. J. Phys. Chem. C **116**, 11413–11425 (2012)
5. F. Lu, W. Cai, Y. Zhang, ZnO hierarchical micro/nanoarchitectures: solvothermal synthesis and structurally enhanced photocatalytic performance. Adv. Funct. Mater. **18**, 1047–1056 (2008)
6. P. Struk, T. Pustelny, K. Gołaszewska, M.A. Borysiewicz, E. Kamińska, T. Wojciechowski et al., ZnO-wide bandgap semiconductor and possibilities of its application in optical waveguide structures. Metrol. Meas. Syst. **21**, 401–412 (2014)
7. Z.L. Wang, J. Song, Piezoelectric nanogenerators based on zinc oxide nanowire arrays. Science **312**, 242–246 (2006)
8. Y. Zeng, T. Zhang, L. Wang, R. Wang, W. Fu, H. Yang, Synthesis and ethanol sensing properties of self-assembled monocrystalline ZnO nanorod bundles by poly(ethylene glycol)-assisted hydrothermal process. J. Phys. Chem. C **113**, 3442–3448 (2009)
9. H. Sun, Y. Yu, J. Luo, M. Ahmad, J. Zhu, Morphology-controlled synthesis of ZnO 3D hierarchical structures and their photocatalytic performance. CrystEngComm **14**, 8626–8632 (2012)
10. Y. Wang, X. Li, N. Wang, X. Quan, Y. Chen, Controllable synthesis of ZnO nanoflowers and their morphology-dependent photocatalytic activities. Sep. Purif. Technol. **62**, 727–732 (2008)
11. A.N. Kadam, R.S. Dhabbe, M.R. Kokate, N.L. Gavade, P.R. Waghmare, K.M. Garadkar, Template free large scale synthesis of multi-shaped ZnO nanostructures for optical, photocatalytical and antibacterial properties. J. Mater. Sci. Mater. Electron. **26**, 8367–8379 (2015)
12. P. Thangaraj, M.R. Viswanathan, K. Balasubramanian, S. Panneerselvam, H.D. Mansilla, M.A. Gracia-Pinilla et al., Morphology controlled synthesis of Sm doped ZnO nanostructures for photodegradation studies of Acid Blue 113 under UV-A light. J. Mater. Sci. Mater. Electron. **26**, 8784–8792 (2015)
13. X. Zhang, J. Pan, C. Zhu, Y. Sheng, Z. Yan, Y. Wang et al., The visible light catalytic properties of carbon quantum dots/ZnO nanoflowers composites. J. Mater. Sci. Mater. Electron. **26**, 2861–2866 (2015)
14. P. Amornpitoksuk, S. Suwanboon, S. Sangkanu, A. Sukhoom, J. Wudtipan, K. Srijan et al., Synthesis, photocatalytic and antibacterial activities of ZnO particles modified by diblock copolymer. Powder Technol. **212**, 432–438 (2011)
15. A.A. Khodja, T. Sehili, J.-F. Pilichowski, P. Boule, Photocatalytic degradation of 2-phenylphenol on TiO2 and ZnO in aqueous suspensions. J. Photochem. Photobiol. A Chem. **141**, 231–239 (2001)
16. A.F. Kohan, G. Ceder, D. Morgan, C.G. Van de Walle, First-principles study of native point defects in ZnO. Phys. Rev. B **61**, 15019–15027 (2000)
17. C. Kormann, D.W. Bahnemann, M.R. Hoffmann, Photocatalytic production of hydrogen peroxides and organic peroxides in

aqueous suspensions of titanium dioxide, zinc oxide, and desert sand. Environ. Sci. Technol. **22**, 798–806 (1988)
18. O.J. Perales-Perez, M.S. Tomar, S.P. Singh, A. Watanabe, T. Arai, A. Kasuya et al., Ambient-temperature synthesis of nanocrystalline ZnO and its application in the generation of hydrogen. Phys. Status Solidi **1**, 803–806 (2004)
19. I. Poulios, I. Tsachpinis, Photodegradation of the textile dye Reactive Black 5 in the presence of semiconducting oxides. J. Chem. Technol. Biotechnol. **74**, 349–357 (1999)
20. S. Sakthivel, B. Neppolian, M.V. Shankar, B. Arabindoo, M. Palanichamy, V. Murugesan, Solar photocatalytic degradation of azo dye: comparison of photocatalytic efficiency of ZnO and TiO2. Sol. Energy Mater. Sol. Cells **77**, 65–82 (2003)
21. S. Gao, S. Jiao, B. Lei, H. Li, J. Wang, Q. Yu et al., Efficient photocatalyst based on ZnO nanorod arrays/p-type boron-doped-diamond heterojunction. J. Mater. Sci. Mater. Electron. **26**, 1018–1022 (2014)
22. J. Li, J. Cao, X. Zhang, S. Wang, Y. Zheng, J. Pan et al., Preparation of cotton cellulose nanofibers/ZnO/CdS nanocomposites and its photocatalytic activity. J. Mater. Sci. Mater. Electron. (2015). doi:10.1007/s10854-015-3914-2
23. B.M. Rajbongshi, A. Ramchiary, B.M. Jha, S.K. Samdarshi, Synthesis and characterization of plasmonic visible active Ag/ZnO photocatalyst. J. Mater. Sci. Mater. Electron. **25**, 2969–2973 (2014)
24. N. Dhiman, B.P. Singh, A.K. Gathania, Synthesis and characterization of dye-doped TiO_2–SiO_2 core-shell composite microspheres. J. Nanophoton. **6**, 063511 (1–10) (2012)
25. J.-M. Herrmann, C. Guillard, P. Pichat, Heterogeneous photocatalysis: an emerging technology for water treatment. Catal. Today **17**, 7–20 (1993)
26. E. Brillas, E. Mur, R. Sauleda, L. Sànchez, J. Peral, X. Domènech et al., Aniline mineralization by AOP's: anodic oxidation, photocatalysis, electro-Fenton and photoelectro-Fenton processes. Appl. Catal. B Environ. **16**, 31–42 (1998)
27. R.K. Dutta, B.P. Nenavathu, S. Talukdar, Anomalous antibacterial activity and dye degradation by selenium doped ZnO nanoparticles. Colloids Surf. B Biointerfaces. **114**, 218–224 (2014)
28. E.K. Goharshadi, Y. Ding, M.N. Jorabchi, P. Nancarrow, Ultrasound-assisted green synthesis of nanocrystalline ZnO in the ionic liquid [hmim][NTf2]. Ultrason. Sonochem. **16**, 120–123 (2009)
29. H. Lu, M. Zhang, M. Guo, Controllable electrodeposition of ZnO nanorod arrays on flexible stainless steel mesh substrate for photocatalytic degradation of Rhodamine B. Appl. Surf. Sci. **317**, 672–681 (2014)
30. K. Prabakar, H. Kim, Growth control of ZnO nanorod density by sol–gel method. Thin Solid Films **518**, 136–138 (2010)
31. M. Pudukudy, Z. Yaakob, Simple chemical synthesis of novel ZnO nanostructures: role of counter ions. Solid State Sci. **30**, 78–88 (2014)
32. N. Uma Sangari, S. Chitra Devi, Synthesis and characterization of nano ZnO rods via microwave assisted chemical precipitation method. J. Solid State Chem. **197**, 483–488 (2013)
33. W.D. Zhou, X. Wu, Y.C. Zhang, M. Zhang, Solvothermal synthesis of hexagonal ZnO nanorods and their photoluminescence properties. Mater. Lett. **61**, 2054–2057 (2007)
34. R. Cuscó, E. Alarcón-Lladó, J. Ibáñez, L. Artús, J. Jiménez, B. Wang et al., Temperature dependence of Raman scattering in ZnO. Phys. Rev. B **75**, 165202 (1–12) (2007)
35. G. Xiong, U. Pal, J.G. Serrano, K.B. Ucer, R.T. Williams, Photoluminesence and FTIR study of ZnO nanoparticles: the impurity and defect perspective. Phys. Status Solidi **3**, 3577–3581 (2006)
36. N. Rana, S. Chand, A.K. Gathania, Tailoring the structural and optical properties of ZnO by doping with Cd. Ceram. Int. **41**, 12032–12037 (2015)
37. J. Tauc, A. Menth, States in the gap. J. Non-Cryst. Solids **8–10**, 569–585 (1972)
38. W. Raza, M.M. Haque, M. Muneer, Synthesis of visible light driven ZnO: characterization and photocatalytic performance. Appl. Surf. Sci. **322**, 215–224 (2014)
39. Y. Fang, Z. Li, S. Xu, D. Han, D. Lu, Optical properties and photocatalytic activities of spherical ZnO and flower-like ZnO structures synthesized by facile hydrothermal method. J. Alloys Compd. **575**, 359–363 (2013)
40. R. Wahab, F. Khan, R.B. Singh, N.K. Kaushik, J. Ahmad, M.A. Siddiqui et al., Utilization of photocatalytic ZnO nanoparticles for deactivation of safranine dye and their applications for statistical analysis. Phys. E Low Dimens. Syst. Nanostruct. **69**, 101–108 (2015)